

HIGH RESOLUTION ANGLE-RESOLVED PHOTOELECTRON SPECTROMETER SYSTEM

A.C. PARR and S.H. SOUTHWORTH

Synchrotron Ultraviolet Radiation Facility, National Bureau of Standards, Washington, DC 20234, USA

J.L. DEHMER

Argonne National Laboratory, Argonne, IL 60439, USA

D.M.P. HOLLAND

Science Research Council, Daresbury Laboratory, Daresbury, Warrington WA4 4AD, UK

The design and construction details for a new high resolution, angle-resolved electron spectrometer system specifically designed for use on the National Bureau of Standards' synchrotron radiation facility (SURF-II) are described. The system features two 10.2 cm mean-radius hemispherical electron energy analyzers in a cryogenically-pumped, magnetically-shielded chamber and may be used to measure vibrationally resolved photoelectron branching ratios and angular distributions from small molecules.

1. Introduction

The many uses of photoelectron spectrometry (PES) with synchrotron radiation (SR) as a light source have been reviewed in the recent literature [1-4]. The general design considerations of the joint use of electron analyzers and SR were reviewed by Smith and Kevan in the previous meeting of this Conference [5]. At the International meeting on Synchrotron Radiation Instrumentation held in Hamburg, Sonntag and Wuilleumier [6] reviewed the types of photoelectron spectrometers currently used for experiments in atomic and molecular physics using SR. A common objective of the various instruments discussed has been the exploitation of the intense, continuous spectral nature of SR to perform differential experiments as a function of photon energy. These efforts have had a major impact in the diverse areas of atomic and molecular physics, surface and solid state science, as well as material and biological studies [7].

The instrument described herein is a second generation electron spectrometer system designed to optimize experimental capability and match the custom monochromators available at the Synchrotron Ultraviolet Radiation Facility (SURF) of the National Bureau of Standards. The first generation apparatus consisted of a single 5 cm mean-radius rotatable analyzer, which had an overall resolution of about 110 meV in typical operation [8]. While adequate for a wide variety of experiments involving simple diatomic molecules [9], this resolution was inadequate to clearly resolve vibrational detail in polyatomic systems, particularly in resonance

regions [10,11]. Moreover, increased sensitivity was needed to examine vibrational and electronic autoionization dynamics within narrow autoionizing resonances [9]. To enable these more sophisticated experiments and to circumvent some of the limitations imposed by the initial design, an entirely new instrument was conceived and its fabrication implemented. After extensive laboratory testing, the instrument is now installed on the normal-incidence beam line at SURF and is undergoing final testing and calibration. An initial report was made on this instrument at the Hamburg meeting [12]. Briefly, the system consists of a 92 cm long, 76 cm diameter triply magnetically-shielded chamber, which is pumped with both a 500 l/s turbopump and a 2000 l/s cryopump. There are two 10.2 cm mean-radius hemispherical electron energy analyzers. One of the analyzers is mounted on a bearing fixture and is rotatable through 120°. The other analyzer remains fixed and monitors electrons along the major polarization axis of the incoming radiation. Fig. 1 shows a schematic of the instrument and most of its major features.

2. Experimental and scientific objectives

The present apparatus is designed to measure photoelectron angular distributions and vibrational branching ratios as a function of photon energy. The basic experimental geometry for angle resolved PES is represented in fig. 2. The photons are supplied via a monochromator such as the 2 m normal-incidence instrument at SURF [13]. The differential cross section in the dipole ap-

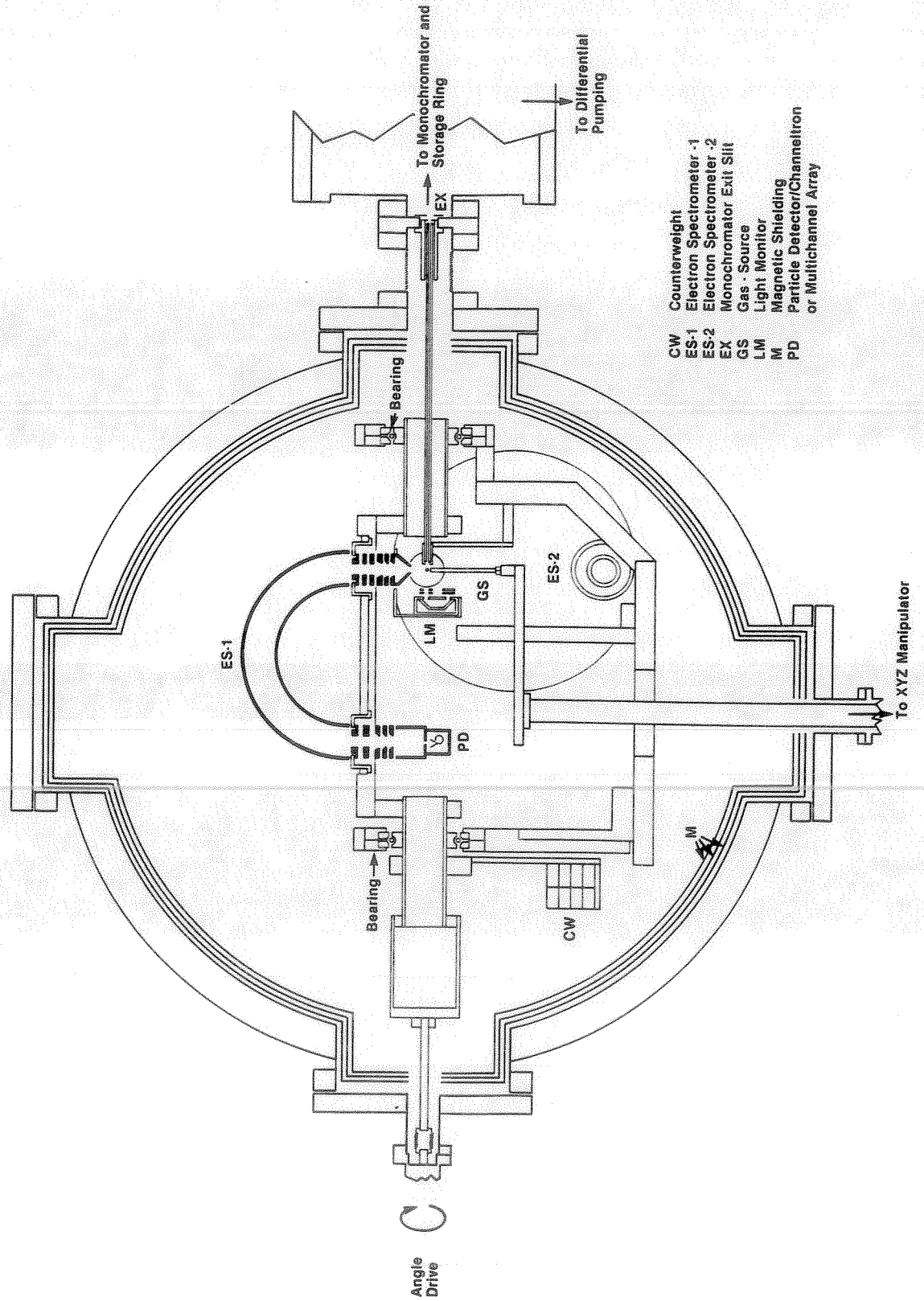


Fig. 1. Schematic of photoelectron spectrometer system and chamber. ES-1 is rotatable through about 120°. ES-2 is fixed and monitors electrons along the major polarization axis of the light.

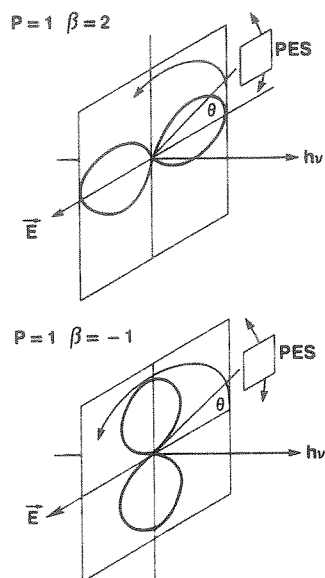


Fig. 2. Schematic of limiting cases of photoelectron angular distributions for randomly oriented atoms or molecules in the dipole approximation. The rotatable photoelectron spectrometer is indicated by the box labeled PES. The electric field vector of the light E is shown perpendicular to the propagation direction of the light on the axis labeled E . For a polarization $P = 1$ (linear polarization) and asymmetry parameter $\beta = 2$, the angular distribution is as shown in the top figure. For $P = 1$ and $\beta = -1$, the distribution is as shown in the bottom portion of the figure.

proximation for photoionization of a randomly oriented gas may be expressed as:

$$\frac{d\sigma_v}{d\Omega} = \frac{\sigma_v}{4\pi} [1 + (\beta_v/4)(3P \cos 2\theta + 1)],$$

where,

- β_v = asymmetry parameter for a vibrational state v ,
- θ = angle of electron ejection with respect to the principal axis of polarization,
- P = polarization of the incoming radiation with the horizontal axis being the major axis,
- σ_v = total cross section for producing vibrational state v of a given electronic state.

The number of electrons ejected per unit light flux per unit solid angle ($dN_v/d\Omega$) is proportional to the differential cross section; hence, we can recast the differential cross section equation directly into measurable quantities:

$$dN_v/d\Omega = N_v [1 + (\beta_v/4)(3P \cos 2\theta + 1)].$$

The solid angle of collection for the device is constant; hence, by measuring the number of electrons as a function of θ and separately determining P , the asymmetry parameter, β_v , and the quantity N_v can be determined. When a number of vibrational transitions are measured,

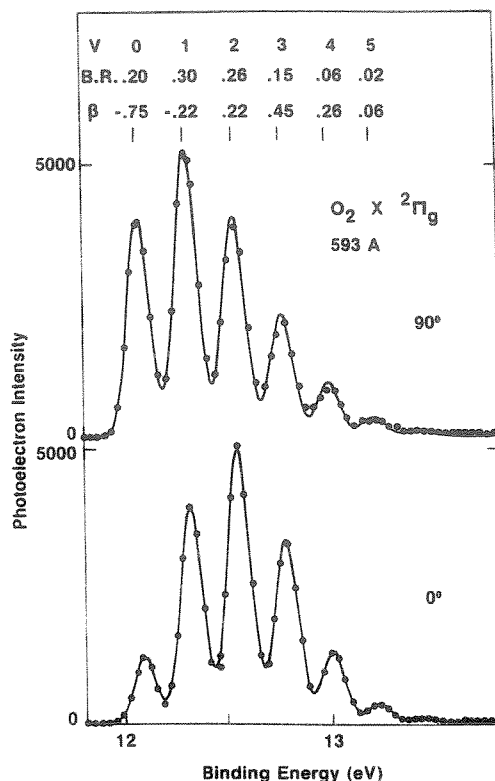


Fig. 3. Sample photoelectron spectra of molecule O_2 showing the vibrationally resolved structure. The branching ratios (BR) and asymmetry parameters are shown at the top.

dividing N_v by the sum over N_v gives the branching ratios within a given electronic transition [14]. Additionally, if the total cross section for an electronic band is known, the partial cross sections for alternative vibrational channels can be obtained.

The type of spectra and information we seek using angle-resolved PES are shown in fig. 3. These spectra were taken with our previous instrument with a combined photon/electron resolution of about 110 meV. Notice that different vibrational peaks display different angular distributions; a hint that this process is being affected by a resonant mechanism. Moreover, these spectra can be accumulated as a function of wavelength, producing wavelength-dependent branching ratios and asymmetry parameters. This information is known to embody the detailed dynamics of resonance phenomena, such as shape resonances and autoionization [9]. Shape resonances result from angular momentum barriers in the molecular field, which give rise to delayed escape of the photoelectron within certain energy ranges. The detailed molecular potential and especially the barrier, are sensitive to molecular geometry and hence, in addition to affecting total absorption cross section, shape resonances can give rise to non-Franck-Condon behavior [9] in the vibrational amplitudes and to vibrational

state dependent variations in the asymmetry parameter within some energy range.

Autoionization, in which a highly excited neutral state decays into the ionization continuum, also gives rise to non-Franck-Condon behavior and to variations in the asymmetry parameters as a function of photon energy and vibrational state. As in the shape resonance phenomena, the photoionization amplitudes for vibrationally resolved transitions may be sensitive to molecular geometry due to the existence of the intermediate autoionizing state. Multichannel Quantum Defect Theory (MQDT) has been used to calculate the branching ratio and asymmetry parameter for molecular hydrogen [9,15,16]. The details of the calculation have yet to be tested experimentally, although excellent agreement has been obtained with the high resolution photoionization data of Dehmer and Chupka [17]. The future extension of such calculations to more complicated molecules is greatly dependent on the availability of high quality experimental data. A major objective of the research made possible by the apparatus described here will be to perform high resolution, i.e. $\Delta E < 50$ meV, photoelectron spectrometry on selected molecules on a fine wavelength mesh. The branching ratios and asymmetry parameters will be determined so as to characterize the detailed dynamics of autoionization processes. This is expected to stimulate additional theoretical work, either with MQDT or new ab initio methods, and to lead to much greater insight into ubiquitous autoionizing resonances in molecular photoionization.

3. Chamber and vacuum system

The vacuum chamber is designed to accommodate a variety of experiments, such as photoion-photoelectron coincidence measurements and various types of fluorescence spectrometers, in addition to the photoelectron spectrometry experiment. The system is modular and will allow for a rapid exchange of experimental instrumentation.

The major design considerations for the vacuum enclosure were:

- 1) accommodate two 10.2 cm mean radius analyzers;
- 2) optimize pumping speed;
- 3) flexibility for exchange of experiment;
- 4) ability to adapt to several monochromators;
- 5) low residual internal magnetic fields.

The first three requirements mandated that the system be large, so as to enable the placement of the electron flight path in the analyzers at a distance of at least 15 cm from the walls, to allow for large and perhaps multiple pumping ports and to provide space for other types of experiments. The size and shape chosen was 92 cm long, 76 cm diameter chamber, oriented such that the light enters perpendicular to the axis

of the cylinder. The vacuum chamber has 84 cm diameter end flanges and eight 25 cm diameter ports for electrical, mechanical and light throughput. One of the large end flanges supports both the mount for the interior apparatus as well as a 30 cm diameter port to attach a cryopump. The cryopump is of the closed-cycle helium refrigerator type, with stated capacity of 2000 l/s for air and 10000 l/s for condensibles such as H₂O. Additional pumping is provided by a 500 l/s turbo molecular pump. The turbo molecular pump is also used for pumping hydrogen and helium, which are pumped ineffectively by the closed-cycle cryopump. The entire chamber is constructed of type 304 stainless steel, with metal-gasket flanges on all ports. The gasket sealing material is copper for the standard 25 cm diameter flanges and gold for the large end flanges. For convenience, the large end flanges also accept a viton seal.

The magnetic shielding is effected with three layers of high permeability alloy material. The outer two layers are 0.75 mm thick and the inner layer is 1.5 mm thick. The spacing between layers is approximately 0.5 cm and is maintained with aluminum spacers. All the side flange ports are also triply shielded with capped inserts and each layer of shielding is terminated with a cap at the large circular ends. Where necessary, holes are punched in the flange cap shielding to accommodate throughputs and to provide for pumping.

The effectiveness of the shielding can be estimated from formulas developed in the literature. The attenuation factor, g , for a single layer of shielding of inner radius r_1 , outer radius r_2 and permeability μ , is given as [18]

$$g = \mu/4 \left[1 - (r_1/r_2)^2 \right].$$

This can be simplified for large diameter, D , and thin shields of thickness, T , to:

$$g = \mu T/D.$$

The factor g is the ratio of the field outside the shielding to the internal field on the axis of the cylinder. In our case, the diameter is 76 cm, with a thickness of 0.75 mm. The magnetic field in the environment of the SURF magnet at the region of the experiment is about 2 G. Under these conditions, standard engineering formulas yield a permeability of $\sim 300\,000$ for the present design. One effective layer of shielding should then give a field on the axis of the chamber of about 6 mG.

At these external fields, the internal field inside the outer shield is ~ 3000 G as can be estimated from [19]

$$B_{\text{int}} \approx 2.5DB_{\text{ext}}/2T.$$

This is a desired range for the outer shield, as the permeability is a maximum for this internal flux range. Two additional inner shields provide further extinction of external fields. The individual attenuation factors for the additional shields are of the order of 30 to 40 each;

hence a combined theoretical attenuation factor of 200 000 or more might be expected. The shielding effectiveness of the inner layers is less, in part, because of the smaller flux densities internal to the shielding, which results in a diminished permeability. A more precise calculation, based upon the method of Sterne [18,20] yields similar values for the total attenuation factors. The measured attenuation factor may be considerably less, due to the approximations made and the imperfect nature of the materials themselves.

In the absence of the spectrometers and their associated mounting hardware, the internal fields were measured to be no larger than several hundred μG . Problems developed, however, when the experimental apparatus, which contained some limited amount of stainless steel, was inserted. Degaussing proved ineffective, since the storage ring magnet ramps several times a day and even the limited leakage through the shield persisted in inducing magnetic behavior in some parts of the apparatus. Additional leakage paths were provided by stainless steel mounting studs and other accessory feedthroughs, which continued from the outer vacuum envelope through the shielding layers. While these fabrication techniques may be tolerated in a laboratory environment, they are not suitable for use in the vicinity of large magnetic fields, such as given by the magnet at

SURF. The best policy is to fabricate using only metals free of ferromagnetic materials. This policy has now been rigorously implemented in the present system, with the resulting return to low internal fields. Other storage rings in general have smaller magnetic fields in the region of the experimental station; however, the alterations in the external field during delivery and installation could aggravate magnetic field problems.

4. Electron spectrometers

Fig. 4 shows a schematic of the electron spectrometers. The entrance and exit lens system are three element zoom lenses after the design of Read [21,22]. They are of the type with an aperture to spacing ratio of 1 and in these units have an image and object distance of five times the aperture diameter. The actual spacing in our case is 0.921 cm. Choosing these parameters, the lens systems can be operated over an order of magnitude variation in kinetic energies around a given pass energy, while retaining unit magnification. The angular acceptance of the entrance lens is set by an aperture in the cone mounted on the first lens element. This aperture, along with its counterpart in the exit image plane, determines the resolution of the instrument. This

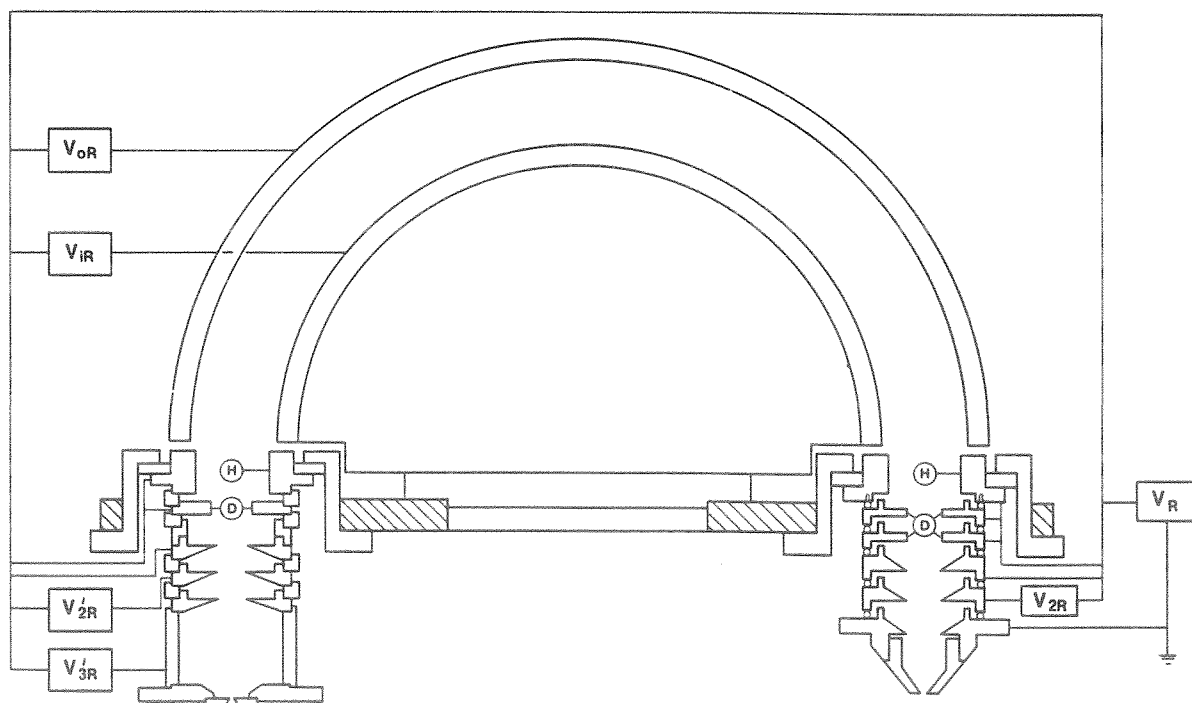


Fig. 4. Details of the photoelectron spectrometer with power supplies shown. Electrodes shown as D are deflectors and electrodes marked H are Herzog correctors. Voltage V_R is the basic reference voltage of the system, referenced to ground. All other lens voltages are measured with respect to V_R , i.e. have their power supply common floating on V_R . They are: V_{2R} focus on entrance lens, V_{OR} and V_{IR} , outer and inner hemisphere potentials, V_{2R} exit lens focus and V_{3R} potential to establish kinetic energy at detector.

arrangement removes the necessity for entrance and exit slits on the hemispherical plane. The fringing fields of the hemisphere are corrected with Herzog [23] electrodes labelled "H" in fig. 4.

The subject of hemispherical analyzers has been covered in the literature [24] in recent years and only those aspects which bear upon the present application will be discussed here. In general, a hemispherical analyzer consists of two concentric hemispheres of inner radius R_i and outer radius R_o . The hemisphere potentials necessary to focus a given energy electron can be found by considering an electron starting at rest, which is accelerated through a potential V to arrive at the normal to the equatorial plane at a kinetic energy expressed in electron volts, $E = V$. The electron will pass through the device along the mean radius $R_m = (R_i + R_o)/2$ if the potential is adjusted to be V along the mean. This requires the inner hemisphere to be at a potential $V_i = V(2R_m/R_i - 1)$ and the outer at $V_o = V(2R_m/R_o - 1)$. To maintain a constant resolution and transmission, as well as for simplicity of operation, it is desirable to keep the pass energy of the analyzer fixed for a given experiment. As a consequence, it is necessary to accelerate or retard the entering electrons as needed, so that their kinetic energy matches the pass energy of the analyzers. An additional constraint is that the entrance cone must be at ground potential, so that the ionization region remains field free.

A schematic of the potential configuration is shown in fig. 5. The total energy of the electron remains fixed and equal to the initial kinetic energy. The various electrode potentials cause changes in the potential energy and corresponding changes in the kinetic energy. The kinetic energy of the electrons on exiting the en-

trance lens is the pass energy, E_a , which is fixed for given experiment. For ease of presentation, it is convenient to refer to fig. 5 for the interplay of kinetic and potential energy. Fig. 5 shows that a reference potential V_R is used to adjust the kinetic energy of the electron to the pass energy, E_a , which determines the potentials of the hemispheres, as in the above analysis. Hence, for varying initial kinetic energies E of the photoelectron the reference voltage V_R must be varied so that

$$E + V_R = E_a,$$

or rewritten

$$E = E_a - V_R.$$

The potentials of the inner and outer hemispheres must then be adjusted by the voltage equivalent of the initial kinetic energy, E , to account for the initial energy of the electron. Hence, for an energy of analysis E_a

$$\begin{aligned} V_o &= E_a(2R_m/R_o - 1) - (E_a - V_R) \\ &= 2E_a(R_m/R_o - 1) + V_R, \end{aligned}$$

$$\begin{aligned} V_i &= E_a(2R_m/R_i - 1) - (E_a - V_R) \\ &= 2E_a(R_m/R_i - 1) + V_R. \end{aligned}$$

It is convenient to measure the potential on the hemispheres with respect to the reference voltage, V_R , then

$$V_{oR} = V_o - V_R = 2E_a(R_m/R_o - 1),$$

$$V_{iR} = V_i - V_R = 2E_a(R_m/R_i - 1).$$

As a consequence of these relationships, the potential of the hemispherical electrodes are a constant value, if they are suitably referenced to the reference potential V_R .

The parameterization of the zoom lens focusing potentials is expressed [21,22] as a function of the ratio of the last electrode voltage to the first, both referenced to the potential at which the electron is at rest. Fig. 5 indicates that this parameterization can be cast in terms of the electron kinetic energy for convenience. For the entrance lens system, the focusing potential on the second electrode, V_{2R} , depends upon the ratio E/E_a and is given by Read [21] and has been checked experimentally. The value of V_{2R} must, of course, take into account that it is referenced to the reference voltage V_R . To achieve best focusing conditions, V_{2R} is under computer control and is varied as a function of photoelectron energy and therefore reference voltage, while scanning a photoelectron spectrum. The exit lens system is somewhat simpler, in that the entrance energy and exit energy are fixed for a given choice of pass energy. The energy of the electron on leaving the exit lens is determined by selecting the kinetic energy of the electron with which the electron hits the detector. A typical value for V_{3R} is 7 V. This procedure allows V_{2R} to be calculated, as well as being checked experimentally. Both lens systems are operated in the mode of unit magnification.

Once the pass energy is selected and the exit lens

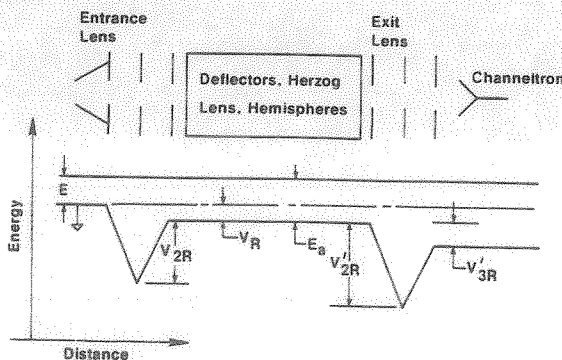


Fig. 5. Schematic of electron spectrometer lens system with an illustrative potential energy plot. The electron is created at the left in a field free region with a kinetic energy E . The electron first enters the entrance lens where it is accelerated by the focusing electrode and subsequently slowed down by the third electrode, such that its kinetic energy is E_a . After dispersion, the electron enters the exit lens system and is focused on the detector.

condition determined, only two voltages, V_{2R} and V_R , need be adjusted to perform a photoelectron energy scan. The kinetic energy, E , which determines V_R is given by

$$E = h\nu - IP,$$

where $h\nu$ is photon energy and IP is the ionization potential of the state under examination. Since $E = (E_a - V_R)$, we can write $V_R = E_a - h\nu + IP$. A precision 16 bit digital to analog power supply under computer control furnishes V_R . All other power supplies are referenced to this voltage.

Deflection electrodes in the position marked D in fig. 4 are used to correct for small misalignments and any residual field effects. One seeks to reduce electric and magnetic fields by adequate shielding, so that all deflection electrodes may be at the potential V_R .

The electrodes, including the hemispheres, are constructed of copper with ceramic or sapphire insulators. The surfaces which are seen by the electrons are coated with colloidal graphite to achieve a uniform surface potential. An electrostatic screening box with apertures for the gas jet and light capillary, encloses the interaction region, to maintain a uniform electric potential in the ionization region. It was found useful to install grounded shields on the entrance lens assemblies and electrode leads, so that electrical fields from these components could not influence the interaction region.

After traversing the analyzer system, the electrons are detected with a continuous channel electron multiplier. The pulses are amplified and accumulated with a computer controlled scaler. A future modification will be to replace the electron multiplier with a microchannel plate/resistive strip area detector. This will permit collecting a range of photoelectron energies simultaneously. An electron of energy $E' = E_a + \Delta E$, will hit the exit plane displaced from the mean radius of the

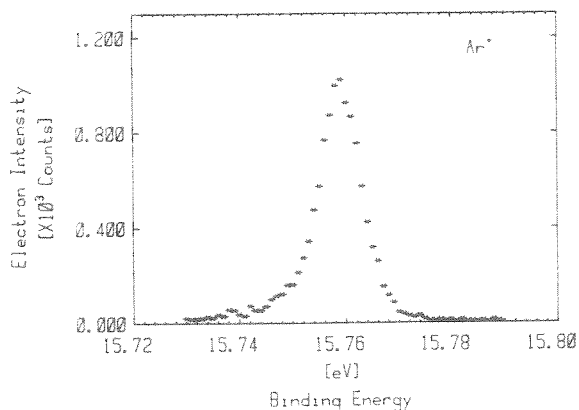


Fig. 6. Photoelectron spectra of the $Ar^+ 2P_{3/2}$ peak taken with a neon resonance line. The pass energy of the analyzer is 1 eV, which results in a resolution of about 9 meV.

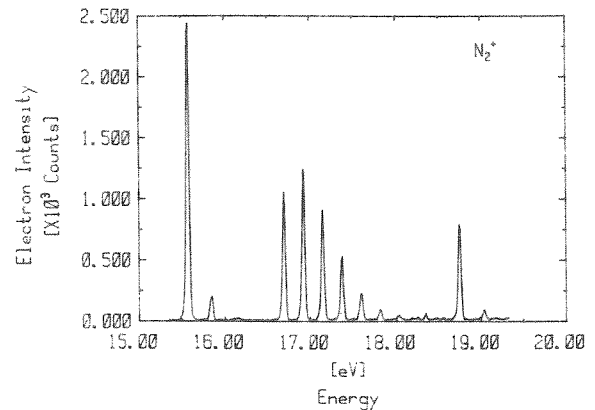


Fig. 7. Photoelectron spectrum of N_2 taken at 5 eV pass energy with the helium resonance lines. The resolution is about 50 meV.

hemispheres by a given amount, X , given by

$$X = 2R_m \Delta E / E_a$$

This equation assumes first order focusing is obtained and will be subject to errors due to higher order aberrations far from the mean radius. The position between the two hemispheres in the exit plane then becomes an energy axis. This can be exploited to achieve greatly enhanced sensitivity [25]. Implementation of this area detector technology is currently underway.

The light intensity and polarization are monitored by the same device as used on our previous apparatus [8], although plans are underway to replace it with a device more mechanically compatible with the new double analyzer system. Briefly, the light monitoring device consists of a 90% transparent tungsten grid followed by 3 glancing angle reflections from gold surfaces to a solid tungsten electrode. The photocurrents from the tungsten electrodes are monitored and the signal differences upon rotation through 90° give the polarization.

Fig. 6 shows a spectrum of argon taken with a laboratory light source emitting the neon resonance lines. The total resolution is 9 meV. Fig. 7 shows a spectrum of N_2 taken with a laboratory light source with 5 V pass energy. The resolution is about 50 meV. These sample data indicate that this system is capable of achieving significantly higher resolution/sensitivity than previously possible with electron spectrometers designed for use with synchrotron radiation.

5. Data acquisition

The entire system is controlled by an LSI 11/23 computer via a CAMAC dataway. The basic reference voltage and sweep are provided by a 16 bit digital to analog converter, which has a range of ± 32 V or ± 110

V, with either a 0.5 mV or 2 mV step resolution. The focus voltages are separately furnished by digital to analog devices through a voltage isolated amplifier. The stepping motor for the monochromator and angle drive are controlled with feedback from absolute shaft encoders. The operator furnishes wavelength, scan and angle parameters, which are used to initiate the data-acquisition cycle. Upon completion of a spectrum at a given wavelength, the photoelectron counts are printed out locally as well as being stored on disk media for subsequent detailed analysis. The time spent at a given point is determined by the integrated light flux; hence, the data come out already corrected for possible light intensity variations. Variants of the main operating system program are used for constant photoelectron energy spectroscopy [26] and for constant initial state spectroscopy. The operating system repeatedly checks for a manual interrupt, which enables the operator to stop an experiment without loss of data. This is useful, for example, for beam reinjection or to avoid temporary changes in beam conditions.

The LSI 11/23 computer is used for data analysis, which can be as simple as summing points, or may involve a complete non-linear least squares analysis with a gaussian basis set. The branching ratios and asymmetry parameters are deduced from measurements at two angles and are frequently compared to a third angle or an independent set of intensity ratios.

The system is calibrated as outlined previously [27] using argon as a sample gas. The argon cross section and asymmetry parameters are known and, along with a set of values for the photoelectric yield of the tungsten detector, give the angle calibration factors and analyzer transmission function. This information is necessary for accurate determination of the asymmetry parameters and branching ratios. The calibration procedure is carried out in varying degrees of complexity at frequent intervals, to ensure the stability of the system.

6. Summary

A photoelectron spectrometer system incorporating two hemispherical analyzers has been tested extensively using a laboratory light source. Fig. 6 shows a spectrum of argon taken using a neon resonance line. With a pass energy of 1 eV and with 0.15 cm entrance and exit apertures, the resolution obtained is about 9 meV. Fig. 7 shows a spectrum of N₂ taken at 5 V pass energy with the helium resonance line. The resolution indicated is about 50 meV, which would be a typical operating condition when the spectrometer is used with synchrotron radiation. The instrument has been installed at SURF and initial testing is underway. The experimental program will begin shortly.

This work was supported in part by the Office of Naval Research, the US Department of Energy and NATO Grant No. 1939.

References

- [1] F.J. Wuilleumier, in *Atomic physics*, vol. 7, eds., D. Klepner and F. Pipkin (Plenum, New York, 1981).
- [2] B.F. Sonntag, in *Recent advances in analytical spectroscopy*, Proc. 9th Int. Conf. on Atomic Spectroscopy, eds., Fuwa and Keiichiro (Pergamon, Oxford, 1982) p. 165.
- [3] *Synchrotron radiation: techniques and applications*, ed., C. Kunz (Springer, New York, Berlin, 1979).
- [4] *Synchrotron radiation research*, eds., H. Winick and S. Doniach (Plenum, New York, 1980).
- [5] N.V. Smith and S.D. Kevan, *Nucl. Instr. and Meth.* 195 (1982) 309.
- [6] B. Sonntag and F. Wuilleumier, *Nucl. Instr. and Meth.* 208 (1983) 735.
- [7] These research endeavors are to some degree summarized in refs. [1-4] as well as in the published Proceedings of the following Conferences:
 - a) Vacuum Ultraviolet VI, Charlottesville, VA, June 2-6, 1980; *Appl. Opt.* 19 (1980).
 - b) Int. Conf. on X-Ray and VUV Synchrotron Radiation Instrumentation, Hamburg, FRG, Aug. 9-13, 1982, *Nucl. Instr. and Meth.* 208 (1983).
 - c) Second Nat. Conf. on Synchrotron Radiation Instrumentation, Ithaca, NY, July 15-17, 1981, *Nucl. Instr. and Meth.* 195 (1982).
- [8] A.C. Parr, R. Stockbauer, B.E. Cole, D.L. Ederer, J.L. Dehmer and J.B. West, *Nucl. Instr. and Meth.* 172 (1980) 357.
- [9] For a review of this work see J.L. Dehmer, D. Dill and A.C. Parr, *Photoionization dynamics of small molecules*, in *Photophysics and Photochemistry in the vacuum ultraviolet*, eds. S.McGlynn, G. Findley and R. Huebner (Reidel, Dordrecht, 1983).
- [10] A.C. Parr, D.L. Ederer, J.L. Dehmer and D.M.P. Holland, *J. Chem. Phys.* 77 (1982) 111.
- [11] A.C. Parr, D.L. Ederer, J.B. West, D.M.P. Holland and J.L. Dehmer, *J. Chem. Phys.* 76 (1982) 4349.
- [12] A.C. Parr, S. Southworth, J.L. Dehmer and D.M.P. Holland, *Nucl. Instr. and Meth.* 208 (1983) 767.
- [13] D.L. Ederer, B.E. Cole and J.B. West, *Nucl. Instr. and Meth.* 172 (1980) 185.
- [14] For a discussion of vibrational amplitudes in electronic transitions see G. Herzberg, *Molecular spectra and molecular structure I, spectra of diatomic molecules* (D. Van Nostrand, Princeton, NJ, 1950). For a discussion of the effects of resonances on the vibrational amplitudes and asymmetry parameters, see ref. [9].
- [15] Ch. Jungen and D. Dill, *J. Chem. Phys.* 73 (1980) 3330.
- [16] M. Raoult and Ch. Jungen, *J. Chem. Phys.* 74 (1981) 3388.
- [17] P.M. Dehmer and W.A. Chupka, *J. Chem. Phys.* 68 (1976) 2243.
- [18] W.G. Wadey, *Rev. Sci. Instr.* 27 (1956) 910.
- [19] Private communication, Mu Shield Company, 121 Madison Street, Malden, MA 02148.
- [20] T.E. Sterne, *Rev. Sci. Instr.* 6 (1935) 324.

- [21] F.H. Read, *J. Phys.* E 3 (1970) 127.
- [22] E. Harting and F.H. Read, *Electrostatic lenses* (Elsevier, Amsterdam, 1976).
- [23] R. Herzog, *Z. Physik* 97 (1935) 596.
- [24] See for example: a) C.E. Kuyatt and J.A. Simpson, *Rev. Sci. Instr.* 38 (1967) 103; b) G.K. Ovrebo and J.L. Erskine, *J. Electron Spectr. Rel. Phen.* 24 (1981) 189; c) H. Wollnik, in *Focusing of charged particles*, ed., A. Septier (Academic Press, New York, 1967); d) D. Roy and J.D. Carette, in *Topics in current physics*, vol. 4, ed. H. Ibach (Springer, Berlin, 1977).
- [25] See for example: a) P.J. Hicks, S. Daviel, B. Wallbank and J. Comer, *J. Phys. E. Sci. Instr.* 13 (1980) 713.
- [26] D.M.P. Holland, J.B. West, A.C. Parr, D.L. Ederer, R. Stockbauer, R.D. Buff and J.L. Dehmer, *J. Chem. Phys.* 78 (1983) 124.
- [27] D.M.P. Holland, A.C. Parr, D.L. Ederer, J.L. Dehmer and J.B. West, *Nucl. Instr. and Meth.* 195 (1982) 331.